

Background Lamb waves in the Earth's atmosphere

Kiwamu Nishida,¹ Naoki Kobayashi,² Yoshio Fukao³

¹ *Earthquake Research Institute, University of Tokyo, Yayoi 1, Bunkyo-ku, Tokyo 113-0032, Japan*

² *Institute of Space and Astronautical Science, Japan Aerospace Exploration Agency,*

3-1-1 Yoshino-dai, Sagami-hara, Kanagawa 229-8510, Japan

³ *Japan Agency for Marine-Earth Science and Technology, 2-15 Natsushima, Yokosuka, Kanagawa 237-0061, Japan*

SUMMARY

Lamb waves of the Earth's atmosphere in the millihertz band have been considered as transient phenomena excited only by large events. Here, we show the first evidence of background Lamb waves in the Earth's atmosphere from 0.2 to 10 mHz, based on the array analysis of microbarometer data from the USArray in 2012. The observations suggest that the probable excitation source is atmospheric turbulence in the troposphere. Theoretically, their energy in the troposphere tunnels into the thermosphere at a resonant frequency via thermospheric gravity wave, where the observed amplitudes indeed take a local minimum. The energy leak through the frequency window could partly contribute to thermospheric wave activity.

Key words: Surface waves and free oscillations, Ionosphere/atmosphere interactions, Atmospheric acoustic-gravity wave

1 INTRODUCTION

Lamb waves of Earth's atmosphere propagate non-dispersively in the horizontal direction with a sound velocity of about 310 m/s, while they are hydrostatically balanced in the vertical direction (Bretherton 1969; Gossard & Hooke 1975; Lindzen 1972). Because the wave energy densities decay exponentially with altitude, they are concentrated in the troposphere. Therefore, these waves are also known as

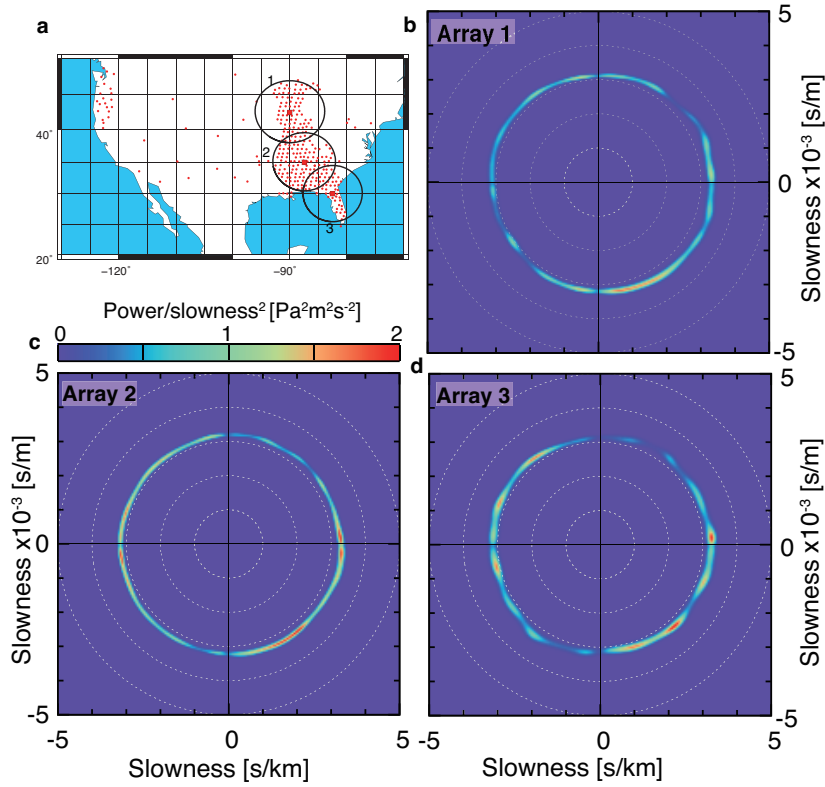


Figure 1. **a**, Location map of the 305 stations used in this study. **b–d**, Results of frequency–slowness spectra at 1.5 mHz. The locations of the subarrays (1–3) are also shown on the map. We averaged the spectra from 1 to 2 mHz for one year. Vertical and horizontal axes show slowness, which is the inverse of the phase velocity.

atmospheric edge waves from Earth’s free surface (Garrett 1969). The Lamb waves in the millihertz band have been considered as transient phenomena excited only by large events (Garrett 1969; Gosard & Hooke 1975) such as the major volcanic eruption of Krakatoa in 1833, the impact of Siberian meteorite in 1908, the testing of large nuclear tests (Donn & Shaw 1967), the 1970 solar eclipse (e.g. Chimonas 1973) and the huge earthquakes (e.g. Mikumo 1968).

In a case of the solid Earth, observation of background free oscillations in the millihertz band—now known as seismic hum (Suda et al. 1998; Kobayashi & Nishida 1998; Nishida 2013), has been firmly established. Above 5 mHz, their dominant excitation sources are oceanic infragravity waves (Rhie & Romanowicz 2004; Webb 2007; Nishida et al. 2008). At 3.7 and 4.4 mHz an elasto–acoustic resonance between the solid Earth and the atmosphere was observed (Nishida et al. 2000). These seismic observations show that the contribution of atmospheric turbulence to the seismic hum is dominant below 5 mHz. Such contribution implies background excitations of atmospheric acoustic–gravity waves, including Lamb waves and acoustic waves, in this frequency range.

For direct detection of the background atmospheric acoustic–gravity waves, our group conducted

observations using an array of barometers (Nishida et al. 2005). However, the spatial scale of the array (~ 10 km) was too small to detect them below 10 mHz. Since then, no direct observations of these waves have been reported. In 2011, 337 high-resolution microbarometers were installed on a continental scale at USArray Transportable Array stations as shown in Fig. 1a (Vernon et al. 2012). The large and dense array enables us to detect the background acoustic–gravity waves.

2 A FREQUENCY–WAVENUMBER SPECTRUM

To detect the background acoustic–gravity waves in the frequency–wavenumber (FK) domain, we calculated an FK spectrum as follows. First, the whole records were divided into about 4.6-h segments. After exclusion of noisy data, cross spectra between every pair of stations were averaged over the remaining data (see Appendix A). Next, the cross spectra were modeled by assuming stationary stochastic excitation of the atmospheric waves by homogeneous and isotropic sources (Nishida et al. 2002). The synthetic cross spectra ϕ can be represented by a superimposition of Legendre functions P_l as a function of separation distance Θ as $\phi(\Theta, f) = \sum_l a_l(f)P_l(\cos \Theta)$. Here, l is the angular order, and the coefficients a_l represent power spectral densities (PSDs) at frequency f . The coefficients a_l were estimated by minimizing the squared differences between the synthetic spectra and the observed ones.

A plot of a_l against angular order l and frequency f gives an FK spectrum as shown in Fig. 2. Their amplitudes are normalized by a reference model for display. Fig. 2 shows a clear branch of Lamb waves with a phase velocity of about 310 m/s from 0.2 to 10 mHz.

Synthetic dispersion curves (see Appendix B) are overlaid on the figure. They show that the observed Lamb-wave branch consists of three sub mode-branches. This is because the Lamb-wave branch intersects that of thermospheric gravity waves at 3.5 mHz and that of acoustic waves trapped near the mesopause at 6.5 mHz (Garrett 1969).

The FK spectrum shows a local minimum of Lamb-wave amplitudes at around 3.5 mHz, where the Lamb-wave branch is crossed by the thermospheric gravity-wave branch. Coupled Lamb waves leak a certain amount of energy from the troposphere to the thermosphere, reducing the Lamb-wave amplitudes at the crossover frequency relative to those at neighboring frequencies, when their excitation sources exist in the troposphere.

Figure 2 also shows a weak branch of first acoustic overtones. The fundamental branch is hardly observable. Their weak amplitudes are partly because most of their modal energy resides in the mesosphere and the thermosphere (Lognonné et al. 1998; Kobayashi 2007; Watada & Kanamori 2010). Moreover, the acoustic modes with lower angular orders (< 200) are too dissipative to keep their excitation amplitudes because the energy radiating into the ionosphere is dissipated via molecular viscosity.

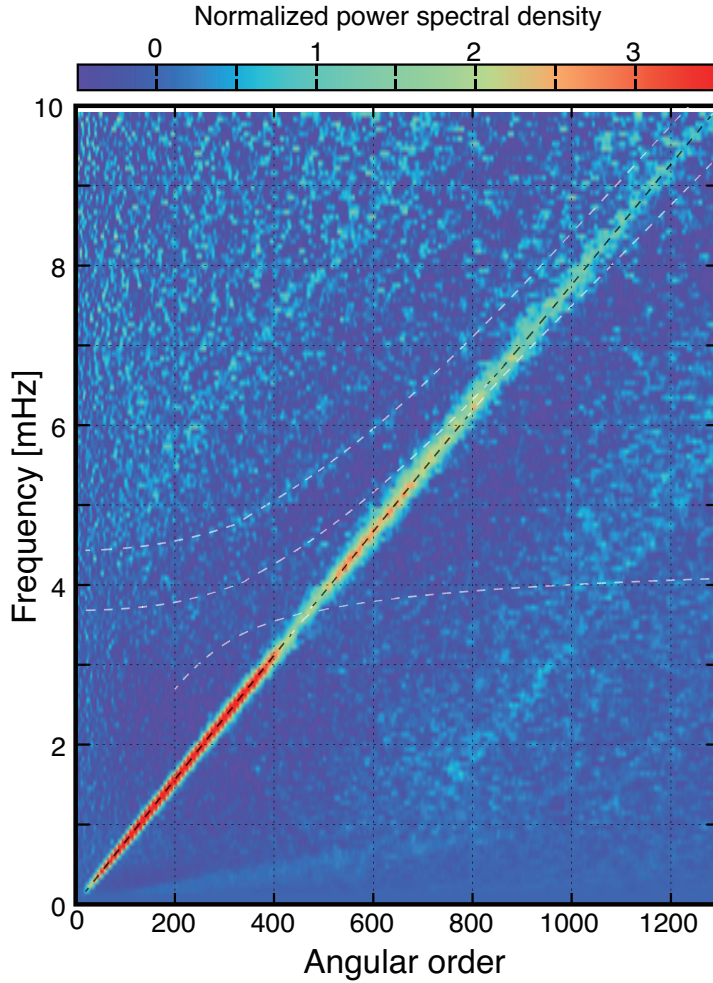


Figure 2. FK spectrum of background Lamb waves. The horizontal axis shows the angular order, and the vertical one shows the frequency in millihertz. The color shows normalized PSDs $a_l/\bar{f}^{-3.5}$, where \bar{f} is the frequency in millihertz. Synthetic dispersion curves are also overlaid on this figure.

3 TWO-DIMENSIONAL FREQUENCY–SLOWNESS SPECTRA

To infer the incident-azimuthal distribution of Lamb waves, we calculated two-dimensional (2-D) frequency–slowness (FP) spectra (Nishida et al. 2005, 2008) at 1.5 mHz (Figs. 1b–d) for the three subarrays. The spectra were obtained by summing the time-delayed cross spectra under the assumption that the background atmospheric waves can be represented by a superimposition of plain waves. Then, the array response functions were deconvolved from the spectra by using the Richardson–Lucy deconvolution algorithm (Lucy 1974; Nishida et al. 2008). Figs. 1b–d show the mean FP spectra from January to November 2012. The spectra clearly show Lamb-wave propagation from all directions. In the figure, the waves are identified as the circle with a slowness of about 3.2 s/km, which is equivalent to a phase velocity of about 310 m/s. The root mean square (RMS) amplitude of these Lamb waves

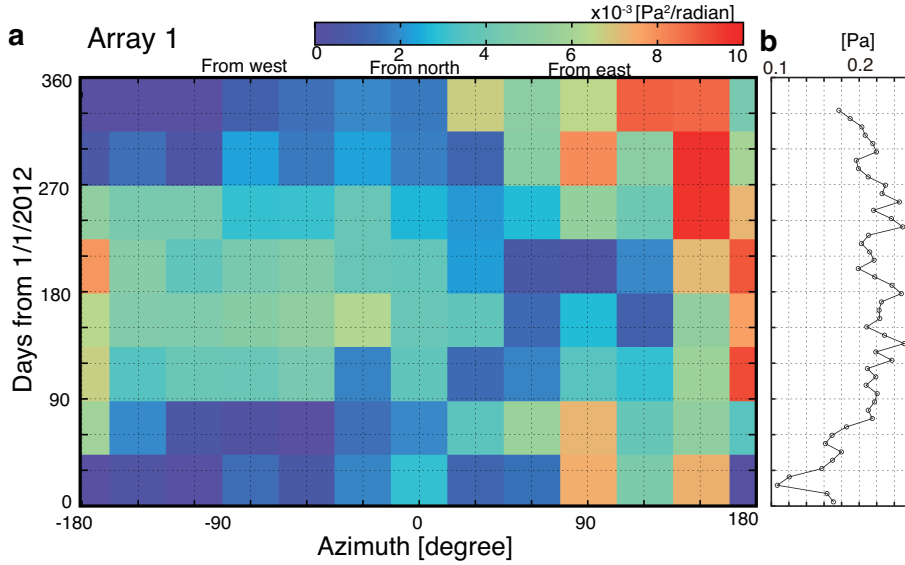


Figure 3. a, Incident-azimuthal variations of Lamb waves of subarray 1 from 1 to 2 mHz every 45 days. Frequency–slowness spectra of subarray 1 were calculated every 45 days. This figure shows their integration with respect to 2-D slowness space every 30 degrees. **b**, Temporal variations of the RMS amplitudes from 1 to 2 mHz every 7 days. The RMS at a time corresponds to the square root of the integration of the FK spectrum (Fig. 2) along the Lamb wave branch.

is about 0.15 Pa. The plots show weak but definite one-lobed anisotropy of the phase velocities. At subarray 1, the phase velocity toward the east is about 20 m/s faster than that toward the west. The anisotropic patterns of subarrays 2 and 3 are similar but smaller than that of subarray 1. The observed anisotropy can be explained by advection attributed to mid-latitude westerlies.

Figure 3a shows the incident-azimuthal variations of Lamb-wave amplitudes at 1.5 mHz as a function of time at an increment of 45 days. Only the result from subarray 1 is shown because most of the stations in subarrays 2 and 3 were installed after April 2012. The figure shows a clear seasonal variation: strong amplitudes from the east side in winter months, and strong amplitudes from the west side in summer months. Primarily, the azimuthal distribution represents their source distribution, although they are also affected by refraction and scattering of the waves owing to topography, wind, and lateral heterogeneities of the sound velocity structure. Because the intrinsic attenuation of Lamb waves is small (i.e., the quality factor is greater than 10^3 , Lindzen 1972), refraction and scattering across long wave paths tend to homogenize the incident-azimuthal distribution.

4 POSSIBLE EXCITATION MECHANISMS

Ocean surface waves at a frequencies around 0.1 Hz excite background seismic surface waves, known as microseisms, and background infrasounds, known as microbaroms (Arendt & Fritts 2000; Donn & Posmentier 1967). During strong storms, strong seismic hum was also observed. For example, an array analysis of USArray records showed seismic signals from Hurricane Irene in 2011 (Traer et al. 2012) including both microseisms (0.03–0.12 Hz) and seismic hum (5–20 mHz). During the observation period in this study, the eastern area of the array was hit by Hurricane Sandy, which excited strong microseisms and microbaroms during the end of October (Hutko 2012). If the oceanic swell is a common source of background Lamb waves, it should also have excited strong Lamb waves during the end of October. For the discussion of the detailed temporal variations, mean RMS amplitudes were also estimated every 7 days with the assumption of their homogeneous and isotropic excitation. Figure 3b shows the RMS amplitudes from 1 to 2 mHz as a function of time. The figure does not show the hurricane-associated activity during the end of October. These results suggest that ocean infragravity waves are not the dominant source.

The atmospheric turbulence in the troposphere is another candidate source of background Lamb waves. Possible physical mechanisms of the atmospheric excitations include aerodynamic excitation by cumulus convection, that associated with generation of cumulus clouds, and that by atmospheric turbulence caused by wave breaking of mountain lee waves. To verify the possibility, we estimate the order of magnitude of Lamb-wave amplitude with angular order $l = 200$ (1.6 mHz) at the surface. We assumed atmospheric sources in the troposphere with two stochastic parameters: (1) the correlation length of 600 m and (2) the PSD of 1.5×10^3 [Pa²/Hz], which were introduced to explain observation of seismic hum below 5 mHz (Kobayashi et al. 2008). The estimated pressure amplitude is of the order of 10^{-2} [Pa] (see Appendix C). This estimation is comparable to the observed one of about 10^{-2} [Pa], which is obtained from the observed FK spectrum (Fig. 2). The parameters are ambiguous because their estimations from the observations are still difficult now. However, this result shows that the atmospheric turbulence is a probable excitation source for the background Lamb waves.

5 DISCUSSIONS

Lamb-wave particle velocity grows with altitude exponentially, although most of the energy resides in the troposphere (Lindzen 1972). Associated atmospheric or ionospheric disturbances in the thermosphere are expected to be detected by other observational methods. To discuss the possibility, we inferred the Lamb-wave particle velocity at different altitudes (Fig. 4) by using eigenfunctions of the Lamb waves (see appendix B). At the surface, they are subjected to a simple power-law decay above

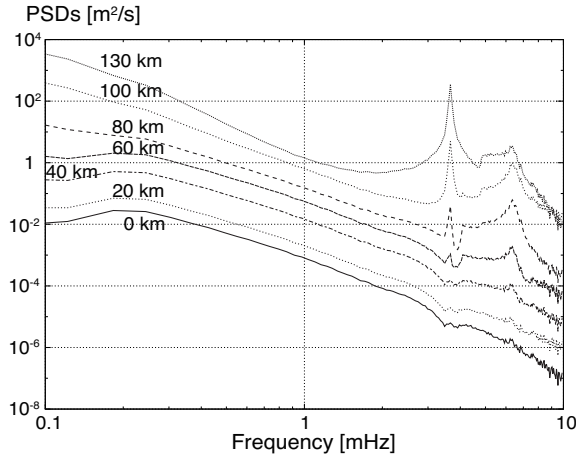


Figure 4. Estimated particle velocity with respect to altitude. Using eigenfunctions of Lamb waves, we inferred the PSDs curves from the surface observation of pressure spectra. At altitudes higher than 60 km, the curves exhibit two resonant peaks, at 3.5 and 6.5 mHz, which are the modes coupled to thermospheric gravity waves and to acoustic waves trapped near the mesopause, respectively.

0.2 mHz, although the figure shows a slight local minimum at 3.5 mHz. The RMS amplitude from 0.2 to 5 mHz reaches the order of 1 m/s at 150 km. At altitudes greater than 60 km, the plot exhibits two peaks at 3.5 and 6.5 mHz, which are the resonant frequencies with the thermospheric gravity waves and the acoustic waves trapped near the mesopause. This figure suggests that the energy tunnels from the troposphere to the thermosphere at the two resonant frequencies, although Lamb waves themselves cannot induce an upward flux (Lindzen 1972). The RMS amplitudes of the two coupled modes reach 0.3 m/s at 150 km and 0.1 m/s at 120 km, respectively. These modes might contribute to the thermosphere energy balance by heating via viscous dissipation (Hickey et al. 2001). The particle velocity from a theoretical model of traveling ionospheric disturbances (TIDs) at 150 km is 5–10 m/s (Kirchengast 1996). The amplitude suggests that the Lamb waves partly contribute to the excitation of small-scale TIDs associated with severe convection activity (Hunsucker 1982).

ACKNOWLEDGMENTS

The data used in this research were obtained from the IRIS Data Management Center. We thank S. Watada for discussion. We also thanks G. Occhipinti and the reviewer for their constructive comments and suggestions. This study is supported by KAKENHI (22740289).

REFERENCES

- Bretherton, F. P., 1969, Lamb waves in a nearly isothermal atmosphere, *Q.J.R. Meteorol. Soc.*, **95** (406), 754–757.
- Chimonas, G., 1973, Lamb waves generated by the 1970 solar eclipse, *Planet. Space Sci.* **21**, 1843–1854.
- Arendt, S. & Fritts, D. C., 2000, Acoustic radiation by ocean surface waves, *J. Fluid Mech.*, **415**, 1–21.
- Dahlen, F.A. & Tromp, J., 1998, *Theoretical Global Seismology*, Princeton: Princeton University Press, 1025 pp.
- Donn, W. L. & Posmentier, E. S., 1967, Infrasonic waves from the marine storm of April 7, 1966, *J. geophys. Res.*, **72**, 2053–2061.
- Donn, W. L. & Shaw, D. M., 1967, Exploring the atmosphere with nuclear explosions, *Rev. Geophys.*, **5** (1), 53–82.
- Fukao, Y., Nishida, K., Suda, N., Nawa, K. & Kobayashi, N., 2002, A theory of the Earth's background free oscillations, *J. geophys. Res.*, **107**, 2206.
- Garrett, C. J. R., 1969, Atmospheric edge waves, *Q. J. R. Meteorol. Soc.*, **95**, 731–753.
- Gossard, EE & Hooke, W. 1975. *Waves in The Atmosphere*. Amsterdam: Elsevier. 442 pp.
- Hickey, M. P., Schubert, G., Walterscheid & R. L., 2001, Acoustic wave heating of the thermosphere, *J. geophys. Res.*, **106**, 21543–21549.
- Hunsucker, R. D., 1982, Atmospheric gravity waves generated in the high-latitude ionosphere: A review, *Rev. Geophys. Space Phys.*, **20**, 293–315.
- Hutko, A., 2012, Effects of Hurricane Sandy visualized across the USArray, *IRIS DMS Newslett.*, **14**.
- Kirchengast, G., 1996, Elucidation of the physics of the gravity wave-TID relationship with the aid of theoretical simulations, *J. geophys. Res.*, **101**, 13353–13368.
- Kobayashi, N. & Nishida, K., 1998, Continuous excitation of planetary free oscillations by atmospheric disturbances, *Nature*, **395**, 357–360.
- Kobayashi, N., 2007, A new method to calculate normal modes, *Geophys. J Int.*, **168**, 315–331.
- Kobayashi, N., Kusumi, T. & Suda, N., 2008, Infrasonds and background free oscillations. *Proc. 8th Int. Conf. on Theoretical and Computational Acoustics, Heraklion, Crete, Greece, 2–5 July 2007*, pp. 105–114, eds. M Taroudakis, P Papadakis. E-MEDIA University of Crete.
- Lindzen, R. S. & Blake, D., 1972, Lamb waves in the presence of realistic distributions of temperature and dissipation, *J. geophys. Res.*, **77**, 2166–2176.
- Lognonné, P., Clévéde, E. & Kanamori, H., 1998, Computation of seismograms and atmospheric oscillations by normal-mode summation for a spherical earth model with realistic atmosphere, *Geophys. J Int.*, **135**, 388–406.
- Lucy, L. B., 1974, An iterative technique for the rectification of observed distributions, *Astron. J.*, **79**, 745–754.
- Mikumo, T., 1968, Atmospheric pressure waves and tectonic deformation associated with the Alaskan earthquake of March 28, 1964, *J. geophys. Res.*, **73** (6), 2009–2025.
- Nishida, K., Kobayashi, N. & Fukao, Y., 2000, Resonant oscillations between the solid Earth and the atmo-

- sphere, *Science*, **287**, 2244–2246.
- Nishida, K., Kobayashi, N. & Fukao, Y., 2002, Origin of Earth’s ground noise from 2 to 20 mHz, *Geophys. Res. Lett.*, **29**, 52-1–52-4.
- Nishida, K., Fukao, Y., Watada, S., Kobayashi, N., Tahira, M., Suda, N., Nawa, K., Oi, T. & Kitajima, T., 2005, Array observation of background atmospheric waves in the seismic band from 1 mHz to 0.5 Hz, *Geophys. J. Int.*, **162**, 824–840.
- Nishida, K. & Fukao, Y., 2007, Source distribution of Earth’s background free oscillations, *J. geophys. Res.*, **112**, B06306 (2007).
- Nishida, K., Kawakatsu, H., Fukao, Y. & Obara, K., 2008, Background Love and Rayleigh waves simultaneously generated at the Pacific Ocean floors, *Geophys. Res. Lett.*, **35**, L16307.
- Nishida, 2013, K. Earth’s background free oscillations, *Annu. Rev. Earth Planet. Sci.* **41**, 719–740.
- Rhie, J. & Romanowicz, B., 2004, Excitation of Earth’s continuous free oscillations by atmosphere–ocean–seafloor coupling, *Nature* **431**, 552–556.
- Picone, J.M., Hedin, A.E., Drob, D.P. & Aikin, A.C., 2002, NRLMSISE-00 empirical model of the atmosphere: Statistical comparisons and scientific issues, *J. geophys. Res.*, **107**, 1468.
- Suda, N., Nawa, K. & Fukao, Y., 1998, Earth’s background free oscillations, *Science*, **279**, 2089–2091.
- Traer, J., Gerstoft, P., Bromirski, P. D. & Shearer, P. M., 2012, Microseisms and hum from ocean surface gravity waves, *J. geophys. Res.*, **117**, B11307.
- Vernon, F., Tytell, J.E., Busby, B., Eakins, J., Hedlin, M., Muschinski, A., Walker, K. & Woodward, B., 2012, Scientific Viability of the USArray Transportable Array network as a real-time weather monitoring platform. Paper presented at 92nd American Meteorological Society Annual Meeting, New Orleans, LA, Am. Meteorol. Soc., 24 January.
- Walterscheid, R.L., Schubert, G. & Brinkman, D.G., 2003, Acoustic waves in the upper mesosphere and lower thermosphere generated by deep tropical convection, *J. geophys. Res.*, **108**, 1392.
- Watada, S. & Kanamori, H., 2010, Acoustic resonant oscillations between the atmosphere and the solid Earth during the 1991 Mt. Pinatubo eruption, *J. geophys. Res.*, **115**, B12319.
- Webb, S. C., 2007, The Earth’s ‘hum’ is driven by ocean waves over the continental shelves, *Nature*, **445**, 754–756.

APPENDIX A: CALCULATION OF CROSS SPECTRA

For the calculation of a cross spectrum, we discarded noisy Fourier components using a typical noise model n of atmospheric pressure at a frequency f (Nishida et al. 2005) as

$$n(f) = 10^{-6} f^{-3} + 10^{-2} [\text{Pa}^2/\text{Hz}]. \quad (\text{A.1})$$

At a frequency f , we thresholded a Fourier spectrum $\tilde{u}_i^k(f)$ of the k th segment at an i th station when $\tilde{u}_i^k(f) > 10 \cdot n(f)$. The threshold can also be represented by weighting the data as $\tilde{u}_i^k(f) w_i^k(f)$, where

the weight of data $w_i^k(f)$ is defined by

$$\begin{aligned} w_i^k(f) &= 1, & \text{if } \tilde{u}_i^k(f) < 10 \cdot n(f), \\ &= 0, & \text{otherwise.} \end{aligned} \quad (\text{A.2})$$

We calculated a weighted cross spectrum $\phi_{ij}(f)$ between the i th station and the j th one as

$$\phi_{ij}(f) = \frac{1}{\sum_k w_i^k(f) w_j^k(f)} \sum_k \tilde{u}_i^k(f) \tilde{u}_j^{k*}(f) w_i^k(f) w_j^k(f). \quad (\text{A.3})$$

APPENDIX B: DISPERSION CURVES AND EIGENFUNCTIONS OF LAMB WAVES

We define eigenfunctions ${}_nU_l$, ${}_nV_l$, and ${}_nX_l$ of an atmospheric mode ${}_nA_l^m(\mathbf{r})$ with a radial order n , an angular order l , and an azimuthal order m as

$${}_n s_l^m(r, \theta, \phi) = {}_n U_l(r) \mathcal{Y}_{lm}(\theta, \phi) \hat{\mathbf{r}} + {}_n V_l(r) \frac{\nabla_l \mathcal{Y}_{lm}(\theta, \phi)}{\sqrt{l(l+1)}}, \quad (\text{B.1})$$

$${}_n p_l^m(r, \theta, \phi) = -{}_n X_l(r) \mathcal{Y}_{lm}(\theta, \phi), \quad (\text{B.2})$$

where ${}_n s_l^m$ is the displacement, ${}_n p_l^m$ is the pressure perturbation, $\hat{\mathbf{r}}$ is a radial unit vector defined on a unit sphere, r is radius, θ is colatitude, ϕ is longitude, \mathcal{Y}_{lm} are real spherical harmonics, and ∇_l is the surface gradient operator (Dahlen & Tromp 1998). For a spherical earth, eigenfunctions and eigenfrequencies ${}_n \omega_l$ are degenerate with respect to azimuthal order m , and the eigenfunctions are functions only of the radius.

Figure A1 shows dispersion curves using globally averaged values over longitude, latitude, and local time based on the atmospheric model NRLMSIS-00 (Picone2002 et al. 2002) in July. In this frequency range at around 3.5 mHz, a physical Lamb-wave branch crosses a physical branch of thermospheric gravity waves. At around 6.5 mHz, a physical Lamb-wave branch crosses a branch of acoustic waves trapped near the mesopause.

Fig. A1 also shows typical eigenfunctions. Eigenfunctions of Lamb waves (${}_0A_{200}$, ${}_0A_{450}$, ${}_1A_{600}$ in the figure) show that the particle motions are almost horizontal and that most of their energy is distributed below 20 km. In contrast, the coupling mode ${}_1A_{450}$ also has energy in the thermosphere at an altitude of 110 km.

With an assumption that the observed pressure perturbations on the surface can be represented by superimposition of eigenfunctions of Lamb modes ${}_n p_l$, we can estimate the particle velocity at ${}_n \omega_l \sqrt{{}_n U_l^2 + {}_n V_l^2}$ as shown in Fig. 4.

To evaluate the excitation amplitudes, we define the modal mass ${}_n M_l$ for a pressure source on the Earth's surface as

$${}_n M_l \sim \frac{\int_0^{R_{top}} 4\pi r^2 \frac{{}_n X_l(r)^2}{\rho(r)\alpha^2(r)} dr}{\frac{{}_n X_l(R)^2}{\rho(R)\alpha^2(R)}}, \quad (\text{B.3})$$

where R_{top} is the radius of the top of the model atmosphere (150 km here), R is the radius of the solid Earth, ρ is the density of the atmosphere, and α is the sound velocity of the atmosphere. This definition shows that the modal mass of the coupled mode is greater than that of non-coupled Lamb modes because of the amplitude in the thermosphere. This means that excitation amplitudes of the coupled mode are expected to be smaller than those for the non-coupled modes when the sources are located in the troposphere.

APPENDIX C: EXCITATION OF LAMB WAVES BY ATMOSPHERIC TURBULENCE

For a quantitative discussion of the force system of the excitation sources, we estimated the excitation amplitude by assuming a random pressure perturbation δp with a coherent length L in the troposphere. We consider pressure disturbances of the turbulence with a coherent volume of $(L \times L \times L)$ (Kobayashi & Nishida 1998; Kobayashi et al. 2008; Walterscheid et al. 2003). A steady-state balance is achieved between the work input from the atmosphere to the mode (the right-hand side) and dissipation of its elastic energy (the left-hand side) as

$$\frac{\omega_l}{Q_l} E_l = (\omega_l \epsilon_l) \delta p L^3 \sqrt{N} \sqrt{2l+1}, \quad (\text{C.1})$$

where Q_l is the modal quality factor, kinetic energy E_l is defined by $(M_l/2)(d_l \omega_l)^2$, strain ϵ_l is $k_l d_l$, the number of turbulent cells N , is $(4\pi R^2)/(L^2)$ with an assumption of a single layer of turbulent cells, $k_l = \sqrt{(l+1)l}/R$ is the wavenumber of the mode, and d_l is the surface displacement of the mode.

Here, we estimate p_{200} with an angular order $l = 200$ at an eigenfrequency of 1.6 mHz. Modal mass ${}_0M_{200}$ was estimated as 8.4×10^{18} kg by using the calculated eigenfunction. An assumed power spectrum of the random pressure is based on an empirical model (Nishida & Fukao 2007; Fukao et al. 2002) as

$$\Psi(f) = 4 \times 10^3 \left(\frac{f}{f_0} \right)^{-2} [\text{Pa}^2/\text{Hz}], \quad (\text{C.2})$$

where the reference frequency $f_0 = 1$ mHz. The pressure forcing of the mode, δp , is estimated by $\sqrt{\Psi \omega_l / Q_l}$. Here, we use typical values of $Q_l = 10^4$ and $L = 600$ m. The surface pressure p_{200} of the Lamb mode is estimated as

$$p_{200} \sim \rho(R) \alpha^2(R) k_{200} d_{200} \sim 1.8 \times 10^{-2} [\text{Pa}], \quad (\text{C.3})$$

where α is the sound velocity at the surface (about 340 m/s). The observed amplitude with angular order 200 (1.6 mHz) is 1.4×10^{-2} [Pa], which was obtained from the FK spectrum (Fig. 2). They are consistent with each other. Because there remain notable ambiguities of correlation length L and quality factor Q_l , more quantitative estimations should be addressed in future studies.

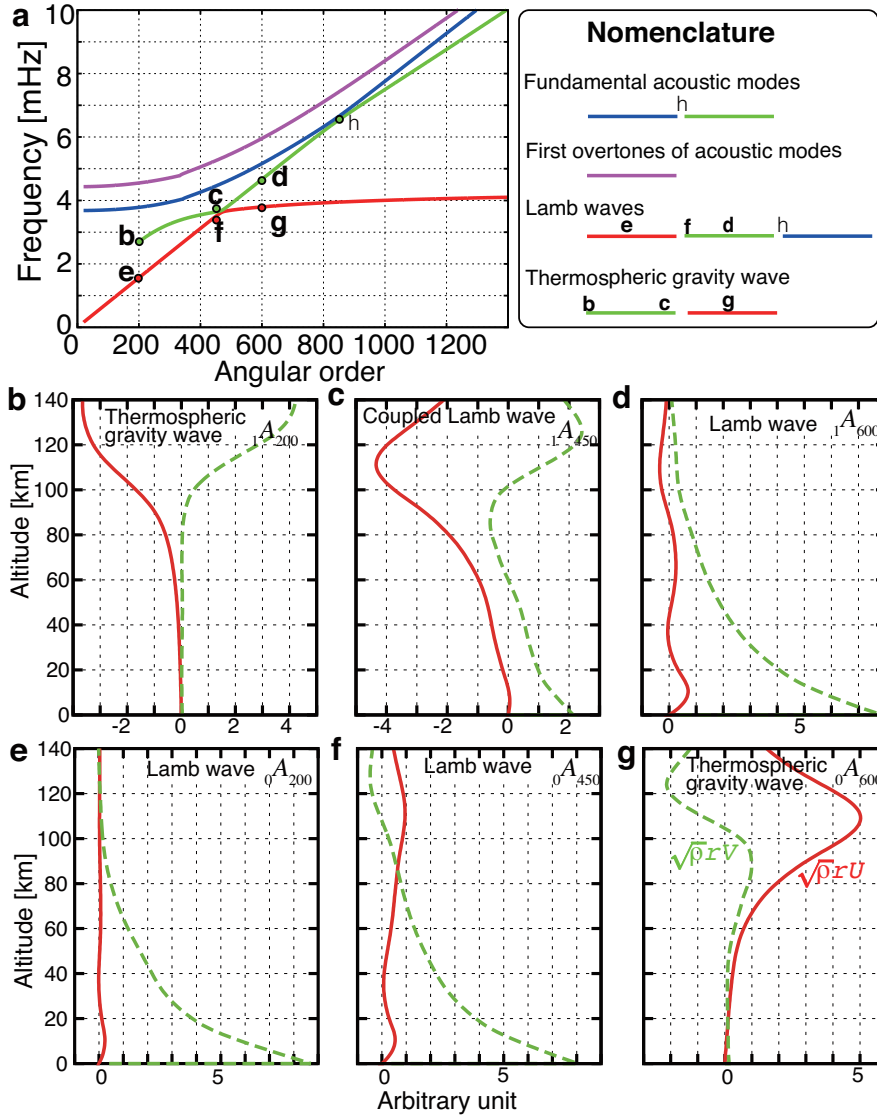


Figure A1. **a**, Dispersion curves and eigenfunctions for the model NRLMSISE-00. We also show nomenclature of the physical branches. **b–g**, Six typical eigenfunctions. Their eigenfrequencies are also shown in **a**. Here we plot only real parts of eigenfunctions, because their amplitudes of the imaginary parts are much smaller than those of the real parts for the following reasons. Lamb waves are trapped near the Earth’s surface. The thermosphere gravity waves also trapped near the mesopause, because they are evanescent at the upper boundary. The dissipation of the modal energy is so small that we can ignore the imaginary parts.

This paper has been produced using the Blackwell Scientific Publications GJI L^AT_EX2e class file.